Spectra and energy levels of Tm^{3+}:$Y_3Al_5O_{12}$

John B. Gruber
Department of Physics, San Jose State University, Washington Square, San Jose, California 95192-0106

Marian E. Hills
Chemistry Division, Naval Weapons Center, China Lake, California 93555-6001

Roger M. Macfarlane
IBM Research Division, Almaden Research Center, 650 Harry Road, San Jose, California 95120-6099

Clyde A. Morrison and Gregory A. Turner
Harry Diamond Laboratories, U.S. Army Adelphi Laboratory Center, 2800 Powder Mill Road, Adelphi, Maryland 20783-1197

Gregory J. Quarles, Gregory J. Kintz,* and Leon Esterowitz
Naval Research Laboratory, Washington, D.C. 20375-5000
(Received 14 June 1989)

Absorption spectra of Tm^{3+}:$Y_3Al_5O_{12}$ are reported between 1.9 and 0.26 μm at 15 and 90 K, and between 0.80 and 0.35 μm at 1.6 K. Laser-excited emission obtained at 80 K is also reported from the Tm^{3+} manifolds $^1D_2$, $^1G_4$, $^3H_4$, and $^3F_4$ to the ground-state manifold, $^3H_6$. The emission from $^1D_2$ also includes transitions to Stark levels in manifolds $^3F_4$, $^3F_3$, and $^3F_2$. Analysis of the emission spectra confirms the experimental crystal-field splitting deduced from an analysis of the hot-band absorption data. Both emission and absorption spectra indicate that Tm^{3+} ions occupy several different sites although the majority of Tm^{3+} ions appear to substitute for Y^{3+} ions in dodecahedral lattice sites (D_2 point-group symmetry). The most intense spectra are analyzed assuming selection rules for D_2 symmetry. A lattice-sum calculation predicts a symmetry of Γ_2 for the ground state. Using this result the symmetries of 20 Γ_1, 11 Γ_2, 17 Γ_3, and 18 Γ_4 Stark levels were identified experimentally and compared with results from a crystal-field splitting calculation. A Hamiltonian consisting of Coulombic, spin-orbit, interconfiguration-interaction, and crystal-field (D_2 symmetry) terms was parametrized and diagonalized for all manifolds of the $Tm^{3+}(4f^{12})$ configuration. The rms deviation between 66 experimental and calculated Stark levels was 11 cm^{-1}.

I. INTRODUCTION

Development of new solid-state lasers, especially those operating between 1.0 and 3.0 μm, has renewed general interest in the optical properties of rare-earth ions (R^{3+}) in yttrium aluminum garnet, $Y_3Al_5O_{12}$ (YAG).[1-12] Spectra and energy levels of several R^{3+} ions that replace Y^{3+} ions in dodecahedral sites in the garnet lattice have been analyzed with success over the past several years.[13-16] Several interpretations have also been advanced to explain additional weak spectra from R^{3+} ions occupying several different sites caused by local strains, or defects due to vacant oxygen sites created during crystal growth.[17,18] Very little has been reported on the spectra and energy levels of Tm^{3+}:YAG.[19-21] Such information is needed for a study of sensitizer-to-activator energy transfer which takes place when Cr^{3+},Tm^{3+}:YAG is used as a laser material.[22,23] A partial listing of levels split by the crystal field has been given for the manifolds $^3H_6$ and $^3F_4$ obtained from fluorescence measurements recorded at 77 K.[20]

This paper presents the absorption spectra of Tm^{3+}:YAG between 1.9 and 0.26 μm at 15 and 90 K, and between 0.80 and 0.35 μm at 1.6 K. Laser-excited emission spectra observed at 80 K are reported from the $^1D_2$ to the $^3H_6$, $^3F_4$, $^3F_3$, and $^3F_2$ manifolds. Confirmation of the crystal-field splitting of the $^3H_6$ manifold is obtained from laser-excited emission from $^3F_4$, $^3H_4$, and $^1G_4$ manifolds. The strongest transitions are used to establish the symmetry labels of the Stark levels of Tm^{3+} ions which substitute for Y^{3+} ions in D_2 sites. The method of analysis has been described earlier.[16] It includes assignment of hot bands observed in absorption and laser-excited fluorescence from specific excited Stark levels. The method assumes that selection rules for D_2 symmetry apply to transitions between Stark levels Γ_1, Γ_2, Γ_3, and Γ_4 of the $^{2S+1}L_J$ manifolds. Experimental levels and their symmetry labels were compared with values calculated using a Hamiltonian consisting of Coulombic, spin-orbit, interconfiguration interaction, and crystal-field terms appropriate to D_2 symmetry. The Hamiltonian was diagonalized for all manifolds of the $4f^{12}$ configuration. By varying the nine crystal-field parameters, B_{km}, we obtained agreement between 66 experimental and calculated Stark levels with a rms deviation of 11 cm^{-1}.

II. EXPERIMENT

Yttrium aluminum garnet melts congruently at 1970 °C. A solid-solution phase exists between the yttrium aluminum garnet and thulium aluminum garnet, $Tm_3Al_5O_{12}$. Single crystals were grown by the Czochralski technique from yttrium aluminum garnet melts doped with thulium oxide in a nitrogen atmosphere containing 1000 ppm of oxygen.[18] Single crystals grew parallel to the ⟨111⟩ direction. Discs were cut parallel to the (111) planes of the crystal. Based on the distribution coefficient of 0.96 and the dopant concentration in the melt, the crystal used for absorption measurements contained approximately 0.08 at. % thulium based on yttrium. The crystal used for the emission spectra contained approximately 0.75 at. % thulium and had dimensions of $8\times8\times11$ mm^3. Both crystals were colorless.

Absorption spectra were measured between 1.9 and 0.26 μm using a Cary Model 2390 spectrophotometer. The instrument has a wavelength calibration feature that compares the wavelength readout against deuterium α and β lines and the α line observed in various orders of the grating. The deviation between the wavelength recorded on the counter and the standard deuterium line was less than 1.5 Å. Resolution better than 1 Å was obtained for most spectra recorded at low temperatures. A spectral bandwidth of 0.4 Å was used in part of the ultraviolet region where sharp peaks having less than 1 Å bandwidth at half-maximum were observed. The precision in measuring the separation between peaks with spectral bandwidths of 1 Å was approximately 0.1 Å. A conduction dewar filled with liquid nitrogen or liquid helium was used to obtain spectra at nominal liquid-nitrogen or liquid-helium temperatures. While sample temperatures were not measured, at least 30 min were allowed for equilibration before data were recorded. From previous experience in taking similar spectra we estimate the crystal temperatures as 90 and 15 K, respectively.

Absorption spectra were also obtained between 0.8 and 0.35 μm using a 1.0-m Czerny-Turner Jarrell-Ash double monochromator with a resolution of 0.2 Å. The sample was immersed in liquid helium and spectra were recorded at 1.6 K. Measured wavelengths were calibrated against the spectrum of neon. The wavelength of the sharpest peaks was determined to better than 0.5 Å. Absorption spectra obtained from the monochromator and the spectrophotometer agreed within ±1 Å.

Emission spectra were recorded between 0.355 and 2.5 μm using a Spex 1.0-m Czerny-Turner monochromator. The resolution of the monochromator was 0.8 cm^{-1}. The sample mounted in a Janis Research Dewar was cooled to 80 K. Emission from the sample was obtained using various excitation sources. The $^1D_2$ manifold was excited at 28 193 cm^{-1} using a Q-switched, frequency-tripled Nd^{3+}:YAG laser. The $^1G_4(\Gamma_3)$ level at 21 227 cm^{-1}, the $^1G_4$ (Γ_1) level at 20 805 cm^{-1}, and the $^3H_4$ (Γ_1) level at 12 607 cm^{-1} were all excited using a tunable dye laser pumped by a Nd^{3+}:YAG laser. The $^3F_4(\Gamma_1)$ level at 5556 cm^{-1} was pumped by a Q-switched Ho^{3+}:YLF laser (where YLF is $YLiF_4$). The pulse widths of the excitation sources were all on the order of nanoseconds, with the associated linewidths typically less than 1 cm^{-1}. Detectors included a cooled photomultiplier tube for ultraviolet and visible emission and a InAs detector for infrared emission.

To avoid interference or saturation from scattered laser light, we gated out the initial few microseconds following excitation and began averaging the signal after the delay. This technique is sound since the lifetimes of the excited Stark levels are on the order of milliseconds while the widths of the excitation pulses are several nanoseconds. To select peak positions we used a center-of-gravity measurement involving the total peak area. The positions of the sharpest peaks were determined with an accuracy better than 1.6 cm^{-1}.

III. METHOD OF ANALYSIS

Yttrium aluminum garnet has cubic space-group symmetry O_h^{10} ($Ia3d$) with eight formula units per unit cell.[24] The lattice-site symmetries of the ions are $Y^{3+}(D_2)$, $Al_1^{3+}(C_{3i})$, $Al_2^{3+}(S_4)$, and $O^{2-}(C_1)$. Tm^{3+} ions that substitute for Y^{3+} ions in the dodecahedral sites experience a crystal field of D_2 symmetry. The D_2 point-group symmetry contains four one-dimensional irreducible representations Γ_1, Γ_2, Γ_3, and Γ_4.[25] Each $Tm^{3+}(4f^{12})$ J-manifold is split into $2J+1$ nondegenerate components (Stark levels). Table I gives the representations for each value of J up to 6. Our calculations predict that magnetic-dipole transitions between Stark levels are usually much weaker than electric-dipole transitions. Table II presents the selection rules for electric-dipole transitions in D_2 symmetry. They are the same for magnetic-dipole transitions with x,y,z referring to the magnetic vector of the light. The analysis of the polarization and site-selective emission from oriented crystals of Tb^{3+}:YAG has been successful in establishing symmetry labels of Tb^{3+} Stark levels.[15] We have also had success in applying an algorithm to the assignment of individual Stark levels[16] which is briefly described here for Tm^{3+}:YAG.

A lattice-sum calculation predicts that the ground state (Z_1) has Γ_2 symmetry. This result is used in the analysis of the absorption and emission spectra. A consistent set of symmetry labels can be assigned to excited Stark levels as follows.

(a) Levels observed in emission from excited Γ_1 Stark levels in $^1D_2$, $^1G_4$, $^3H_4$, and $^3F_4$ have either Γ_2, Γ_3, or Γ_4 symmetry; levels established from other measurements,

TABLE I. Full-rotation compatibility table for the D_2 group.

J	Γ_1	Γ_2	Γ_3	Γ_4
0	1	0	0	0
1	0	1	1	1
2	2	1	1	1
3	1	2	2	2
4	3	2	2	2
5	2	3	3	3
6	4	3	3	3
$Tm^{3+}(4f^{12})$ Total	28	21	21	21

TABLE II. Electric-dipole selection rules for D_2 symmetry.

	Γ_1	Γ_2	Γ_3	Γ_4
Γ_1		y	z	x
Γ_2	y		x	z
Γ_3	z	x		y
Γ_4	x	z	y	

but absent in emission from Γ_1 levels have Γ_1 symmetry. The absence of a 27-cm^{-1} hot band in the absorption spectrum of the $^3P_0(\Gamma_1)$ suggests that Z_2, the first excited Stark level above the ground state, has Γ_1 symmetry. The absence of emission from excited Γ_1 levels to the 27-cm^{-1} level supports this assignment. The absence of emission from excited Γ_1 levels to Z_6 at 252 cm^{-1} indicates that Z_6 has Γ_1 symmetry.

(*b*) Assuming Z_1 has Γ_2 symmetry, levels observed in the 1.6-K absorption spectrum have Γ_1, Γ_3, or Γ_4 symmetry. If these levels lack a hot band at 27 cm^{-1}, they have Γ_1 symmetry; if they have a 27-cm^{-1} hot band, they have either Γ_3 or Γ_4 symmetry.

(*c*) Levels observed in emission from excited Γ_3 Stark level ($^1D_2$, $^1G_4$) have symmetry Γ_1, Γ_2, or Γ_4. Levels observed in emission from excited Γ_1 states not observed in emission from excited Γ_3 states are assigned Γ_3 symmetry.

(*d*) Excited Γ_2 Stark levels can be located by observing isolated pairs of hot bands in absorption separated by 189 cm^{-1}, and inferring the energy of the forbidden $\Gamma_2 \rightarrow \Gamma_2$ transition.

(*e*) Hot bands from Stark levels Z_2, Z_3, and Z_5 or from levels Z_2, Z_4, and Z_5 to excited Stark levels observed at 1.6 K indicate that the excited Stark level has the same symmetry as Z_4 or Z_3, respectively. Hot-band sequences from levels Z_3 and Z_4 plus emission to the $^3H_6$ manifold establish Z_3 with Γ_4 symmetry and Z_4 with Γ_3 symmetry.

IV. ABSORPTION SPECTRA

Table III presents the absorption observed at approximately 15 K. Temperature-dependent peaks (hot bands) were confirmed by comparison with spectra obtained at 90 K. Absorption spectra of the $^3H_4$, $^3F_3$, $^3F_2$, $^1G_4$, and $^1D_2$ manifolds were also recorded at 1.6 K; peaks persisting at 1.6 K are identified in Table III. Figures 1–8 present the spectra of the $^3H_4$, $^3F_3$, $^1G_4$, $^1D_2$, $^1I_6$, $^3P_0$, $^3P_1$, and $^3P_2$ manifolds at 1.6 and 15 K. Only the most intense bands or lines were analyzed as representative of Tm^{3+} ions in sites of D_2 symmetry. More than 150 hot bands establish excited Stark levels, Z_2 at 27 cm^{-1}, Z_3 at 216 cm^{-1}, Z_4 at 241 cm^{-1}, Z_5 at 247 cm^{-1}, and Z_6 at 252 cm^{-1}. These levels are in agreement with levels deduced from the emission data. Table III also includes the method of assignment of symmetry labels to Stark levels based on the algorithm given in the previous section.

From the number of observed peaks associated with each $^{2S+1}L_J$ manifold it is clear that Tm^{3+} ions occupy several minority sites. A close look at Fig. 4, for example, reveals a number of weak absorption peaks clustered around a strong, sharp peak. The spectrum of $^3F_3$ (Fig. 2) contains a number of weak to moderately strong peaks, in addition to those expected for Tm^{3+} ions in a single site. The peaks retain their relative strength at two different concentrations and hence are not thought to be associated with pairs or clusters of Tm^{3+} ions.

Throughout the entire spectrum each observed manifold includes several sharp intense peaks at 1.6 and 15 K whose hot bands observed at 90 K predict levels Z_2 through Z_6 within ± 2 cm^{-1}. The energy of these strong peaks was assigned to the energy-level scheme for Tm^{3+} ions in D_2 sites. Absorption peaks observed at 1.6 and 15 K become increasingly sharp toward the low-energy side of each manifold since the higher energy levels are broadened by spontaneous phonon emission which is typical of solid-state rare-earth ion spectra. Multiphonon absorption due to the garnet lattice appears below 2200 cm^{-1}.

V. LASER-EXCITED EMISSION SPECTRA

Figure 9 shows the 80-K emission from the lowest Stark level in $^3F_4$, identified as a Γ_1 level in absorption, to the various Stark levels of the ground-state manifold, $^3H_6$. Strong emission peaks, two of which have well-defined shoulders, establish terminal levels at 220, 241, 247, 588, and 610 cm^{-1}. The 220-, 241-, and 247-cm^{-1} values are within experimental error of the Stark levels deduced from hot-band absorption data (Table III). The crystal lases from the $^3F_4(\Gamma_1)$ Stark level to levels at 247, 588, and 610 cm^{-1}. Weaker, broader bands with structure are also observed in Fig. 9 and very likely represent phonon sidebands together with possible weak electronic transitions. We have not made a distinction between purely electronic and phonon sidebands associated with the weaker emission appearing in Fig. 9.

Table IV lists the 80-K emission from $^3F_4(\Gamma_1)$ at 5556 cm^{-1} to the $^3H_6$ manifold. The splitting deduced from the emission data is compared with the Stark levels established from the absorption data and levels predicted by the crystal-field splitting calculation presented in Table V. If we assume that the ground-state level has Γ_2 symmetry, then from the analysis of the absorption spectra the energy levels up to 252 cm^{-1} can be assigned the symmetry labels shown in column 7 and compared with predicted labels shown in column 8. The absence of emission to levels identified as Γ_1 in absorption and predicted as Γ_1 by the calculation indicates a consistency in the analysis. The strong emission peak and shoulder used to establish terminal Stark levels at 588 and 610 cm^{-1} represent electronic transitions to levels having Γ_2, Γ_3, or Γ_4 symmetry. Since two of a possible three Γ_2 labels for a $J=6$ manifold have already been assigned, we expect that both levels cannot have Γ_2 symmetry. The calculation (Table V) predicts a Γ_4 at 518 cm^{-1} and a Γ_3 at 610 cm^{-1}. Small changes in B_{km} parameters can improve agreement between calculated and observed levels. However, the emission data are not sufficient to establish independently the symmetry of each of these two experimental levels. The broad band at 690 cm^{-1} may contain

TABLE III. Absorption spectrum of Tm^{3+}:$Y_3Al_5O_{12}$; spectrum was recorded at approximately 15 K.

$^{2S+1}L_J$	λ (Å)[a]	I	E (cm^{-1})[b]	Trans.[c]	E (cm^{-1})[d]	Γ_n^e
$^3F_4$	18 810*	0.02	5315	$Z_4 \rightarrow Y_1$	241	
	18 719*	0.02	5340	$Z_3 \rightarrow Y_1$	216	
	18 210*	0.02	5489	$Z_5 \rightarrow Y_2$	247	
	18 110*	0.02	5521	$Z_3 \rightarrow Y_2$	215	
	17 994	0.05	5556	$Z_1 \rightarrow Y_1$	0	1(*b,c*)
	17 915*	0.02	5580	$Z_6 \rightarrow Y_3$	252	
	17 879*	0.02	5592	$Z_4 \rightarrow Y_3$	240	
	17 800*	0.02	5617	$Z_3 \rightarrow Y_3$	215	
	17 682*	0.02	5654	$Z_5 \rightarrow Y_4$	247	
	17 663*	0.03	5660	$Z_4 \rightarrow Y_4$	241	
	17 510*	0.04	5709	$Z_2 \rightarrow Y_2$	27	
	17 432	0.57	5736	$Z_1 \rightarrow Y_2$	0	3(*a,b,c*)
	17 400	0.02	5746			
	17 254*	0.03	5794	$Z_5 \rightarrow Y_5$	247	
	17 235*	0.04	5801	$Z_4 \rightarrow Y_5$	240	
	17 222*	0.23	5805	$Z_2 \rightarrow Y_3$		
			(5832)	(Y_3)		2(*a,c,d*)
	17 165*	0.02	5825	$Z_3 \rightarrow Y_5$	216	
	17 073*	0.02	5856			
	17 019*	0.09	5874	$Z_2 \rightarrow Y_4$	27	
	16 690*	0.02	5891	$Z_3 \rightarrow Y_6$	217	
	16 942	0.94	5901	$Z_1 \rightarrow Y_4$	0	4(*a,b,c*)
	16 924	0.02	5907			
	16 878*	0.14	5923	$Z_5 \rightarrow Y_7$	247	
	16 860*	0.04	5929	$Z_4 \rightarrow Y_7$	241	
	16 800*	0.02	5954	$Z_3 \rightarrow Y_7$	216	
	16 550	0.06	6041	$Z_1 \rightarrow Y_5$	0	1(*b,c*)
	16 441*	0.02	6081	$Z_2 \rightarrow Y_6$		
			(6108)	(Y_6)		2(*a,c,d*)
	16 274	0.85	6143			
	16 203	0.93	6170	$Z_1 \rightarrow Y_7$	0	1(*b,c*)
	16 133*	0.02	6197	$Z_2 \rightarrow Y_8$	27	
	16 110*	0.02	6206	$Z_2 \rightarrow Y_9$	27	
	16 060	0.13	6224	$Z_1 \rightarrow Y_8$	0	
	16 040	0.02	6233	$Z_1 \rightarrow Y_9$	0	
	16 020	0.01	6240			
$^3H_5$	12 355*	0.02	8092	$Z_5 \rightarrow X_1$	247	
	12 345*	0.04	8098	$Z_5 \rightarrow X_2$	247	
				or $Z_4 \rightarrow X_1$	241	
	12 297*	0.02	8130	$Z_3 \rightarrow X_2$	215	
	12 098*	0.04	8264	$Z_6 \rightarrow X_3$	252	
	12 090*	0.04	8269	$Z_5 \rightarrow X_3$	247	
	12 070*	0.03	8283	$Z_5 \rightarrow X_4$	247	
	12 060*	0.02	8290	$Z_4 \rightarrow X_4$	240	
	12 044*	0.03	8300	$Z_3 \rightarrow X_3$	216	
	12 028*	0.06	8312	$Z_2 \rightarrow X_1$	27	
	12 022*	0.04	8315	$Z_3 \rightarrow X_4$	215	
	12 019*	0.05	8318	$Z_2 \rightarrow X_2$	27	
	12 007	0.02	8326			
	11 988	0.09	8339	$Z_1 \rightarrow X_1$	0	4(*b,e*)
	11 980	0.08	8345	$Z_1 \rightarrow X_2$	0	3(*b,e*)
	11 901	0.01	8400			
	11 812	0.02	8464			
	11 778*	0.80	8489	$Z_2 \rightarrow X_3$	27	
	11 739	0.78	8516	$Z_1 \rightarrow X_3$	0	3(*b,e*)
	11 720	0.64	8530	$Z_1 \rightarrow X_4$	0	1(*b,e*)
	11 718(sh)*	0.10	8531	$Z_2 \rightarrow X_6$		
	11 684	0.81	8556	$Z_1 \rightarrow X_6$	0	4(*b*)
	11 640	0.01	8589			
	11 610	0.01	8611			
	11 600	0.01	8618			

TABLE III. (*Continued*).

$^{2S+1}L_J$	λ (Å)[a]	I	E (cm^{-1})[b]	Trans.[c]	E (cm^{-1})[d]	Γ_n^e
	11 516*	0.04	8684	$Z_2 \rightarrow X_7$	27	
			(8711)	(X_7)		2(*d*,*e*)
	11 396[f]	0.02	8773	$Z_1 \rightarrow X_8$	0	
	11 360[f]	0.04	8800	$Z_1 \rightarrow X_9$	0	
	11 290*	0.01	8855	$Z_2 \rightarrow X_{11}$	27	
	11 256[f]	0.03	8882	$Z_1 \rightarrow X_{11}$	0	
$^3H_4$	8083.0*	0.02	12 367	$Z_4 \rightarrow W_1$	240	
	8068*	0.02	12 392	$Z_3 \rightarrow W_1$	215	
	8038.0*	0.02	12 439	$Z_4 \rightarrow W_2$	240	
	8023.5*	0.02	12 461	$Z_3 \rightarrow W_2$	215	
	7994*	0.03	12 506	$Z_4 \rightarrow W_3$	241	
	7932.6[g]	0.02	12 604			
	7931.1[g]	0.06	12 605			
	7930.0[g]	0.55	12 607	$Z_1 \rightarrow W_1$	0	1(*b*,*e*)
	7928*	0.03	12 610	$Z_3 \rightarrow W_5$	214	
	7925.4[g]	0.02	12 614			
	7922.4[g]	0.07	12 619			
	7912.0*	0.02	12 636	$Z_3 \rightarrow W_5$	215	
	7907.0[g]	0.02	12 644			
	7902.0[f]	0.02	12 652	$Z_2 \rightarrow W_2$	27	
	7885.0	0.01	12 679	$Z_1 \rightarrow W_2$	0	2(*d*,*e*)
	7869.0[f,g]	0.05	12 705			
	7859.8*	0.80	12 720	$Z_2 \rightarrow W_3$	27	
	7855.7[g]	0.05	12 726			
	7848.5[g]	0.02	12 738			
	7845.4[g]	0.06	12 743			
	7842.6[g]	0.69	12 747	$Z_1 \rightarrow W_3$	0	4(*b*,*e*)
	7813.0*	0.14	12 797	$Z_2 \rightarrow W_5$	27	
	7796.0[g]	0.44	12 824	$Z_1 \rightarrow W_5$	0	3(*b*,*e*)
	7771.0[g]	0.02	12 865			
	7736*	0.02	12 922	$Z_3 \rightarrow W_8$	217	
	7702.0[g]	0.02	12 980			
	7698.0[g]	0.02	12 989			
	7685.0[f,g]	0.02	13 009			
	7664.0*	0.04	13 045	$Z_2 \rightarrow W_7$		
	7656.0[f,g]	0.02	13 058			
	7648.0[g]	0.04	13 072	$Z_1 \rightarrow W_7$	0	4(*b*,*e*)
	7642.0[f,g]	0.04	13 082			
	7632.4	0.04	13 098			
	7624.5*	0.03	13 112	$Z_2 \rightarrow W_8$	27	
	7608.0[g]	0.04	13 139	$Z_1 \rightarrow W_8$	0	3(*b*)
	7604.0[f,g]	0.02	13 147			
	7597.0[g]	0.08	13 159	$Z_1 \rightarrow W_9$	0	
	7592.0[g]	0.01	13 168			
$3F_3$	6937.0*	0.01	14 412	$Z_5 \rightarrow V_1$	247	
	6933.0*	0.01	14 420	$Z_4 \rightarrow V_1$	239	
	6926.5*	0.02	14 432	$Z_5 \rightarrow V_2$	247	
	6917.3*	0.02	14 453			
	6912*	0.04	14 463	$Z_3 \rightarrow V_2$	216	
	6905.0*	0.02	14 479			
	6903.9*	0.07	14 480	$Z_4 \rightarrow V_5$	240	
	6893.8*	0.03	14 502	$Z_4 \rightarrow V_6$	239	
	6883.0*	0.03	14 525	$Z_3 \rightarrow V_6$	216	
	6832.6*	0.80	14 632	$Z_2 \rightarrow V_1$	27	
	6827.4*	0.20	14 644			
	6825.0[g]	0.10	14 648			
	6832.2*	0.70	14 652	$Z_2 \rightarrow V_2$	27	
	6820.0[g]	1.20	14 659	$Z_1 \rightarrow V_1$	0	4(*a*,*b*,*c*)
	6816.0[g]	0.10	14 666			
	6814.1[g]	0.20	14 671			

TABLE III. (*Continued*).

$^{2S+1}L_J$	λ (Å)[a]	I	E (cm^{-1})[b]	Trans.[c]	E (cm^{-1})[d]	Γ_n^e
	6810.4[g]	1.70	14 679	$Z_1 \rightarrow V_2$	0	3(*a*,*b*,*c*)
	6806.1[g]	0.10	14 689			
	6801.0[g]	0.10	14 699			
	6798.4[g]	1.56	14 705	$Z_1 \rightarrow V_4$	0	
	6793.9[g]	0.05	14 715			
	6791.5[g]	0.80	14 720	$Z_1 \rightarrow V_5$	0	
	6789.6*	0.04	14 724			
	6782.2[g]	0.14	14 741	$Z_1 \rightarrow V_6$	0	1(*b*,*c*)
	6779.4[g]	0.04	14 746			
	6768.6[g]	0.03	14 770			
$^3F_2$	6665.7*	0.03	14 998	$Z_5 \rightarrow U_1$	247	
	6657.1*	0.03	15 017	$Z_5 \rightarrow U_2$	247	
	6654.5*	0.02	15 023	$Z_4 \rightarrow U_2$	241	
	6651.5*	0.02	15 029	$Z_3 \rightarrow U_1$	216	
	6569.0*	0.01	15 218	$Z_2 \rightarrow U_1$	27	
	6561.3*	0.04	15 237	$Z_2 \rightarrow U_2$	27	
	6557.8[g]	0.06	15 245	$Z_1 \rightarrow U_1$	0	3(*a*,*b*,*c*)
	6549.3[g]	0.29	15 264	$Z_1 \rightarrow U_2$	0	4(*a*,*b*,*c*)
	6510.4	<0.01	15 356			
	6492.0	0.02	15 403			
	6479.0[g]	<0.01	15 430			
	6475.9[g]	0.04	15 438	$Z_1 \rightarrow U_5$	0	1(*b*,*c*)
$^1G_4$	4863*	0.01	20 558	$Z_5 \rightarrow A_1$	247	
	4861.2*	0.01	20 565	$Z_4 \rightarrow A_1$	240	
	4855.5*	0.02	20 590	$Z_3 \rightarrow A_1$	215	
	4805.3[g]	0.11	20 805	$Z_1 \rightarrow A_1$	0	1(*b*,*c*)
	4765.0*	0.02	20 980	$Z_5 \rightarrow A_3$	247	
	4757.8*	0.02	21 011	$Z_3 \rightarrow A_3$	216	
	4715.7*	0.13	21 200	$Z_2 \rightarrow A_3$	27	
	4709.6[g]	0.11	21 227	$Z_1 \rightarrow A_3$	0	3(*b*,*e*)
	4681.6*	0.03	21 354	$Z_2 \rightarrow A_4$	27	
	4675.6[g]	0.05	21 381	$Z_1 \rightarrow A_4$	0	4(*b*,*e*)
	4661.5*	0.02	21 446	$Z_4 \rightarrow A_6$	241	
	4656.0*	0.03	21 472	$Z_3 \rightarrow A_6$	215	
	4643.4[g]	0.05	21 530	$Z_1 \rightarrow A_5$	0	1(*b*,*e*)
	4615.2*	0.04	21 660	$Z_2 \rightarrow A_6$	27	
			(21 687)	(A_6)		2(*d*,*e*)
	4603.3[g]	0.03	21 717			
	4595.0[g]	0.40	21 757	$Z_1 \rightarrow A_7$	0	1(*b*,*e*)
	4595.0*	0.30	21 757	$Z_2 \rightarrow A_8$	28	
	4589.0[g]	0.30	21 785	$Z_1 \rightarrow A_8$	0	
$^1D_2$	3619.4*	0.02	27 621	$Z_5 \rightarrow B_1$	247	
	3618.5*	0.03	27 628	$Z_4 \rightarrow B_1$	240	
	3618.1*(sh)	0.03	27 630	$Z_5 \rightarrow B_2$	247	
	3615.2*	0.02	27 652	$Z_3 \rightarrow B_1$	216	
	3614.0*	0.02	27 662	$Z_3 \rightarrow B_2$	215	
	3598.4*	0.02	27 782	$Z_4 \rightarrow B_3$	241	
	3596.5*	0.03	27 797	$Z_5 \rightarrow B_4$	247	
	3596(sh)*	0.03	27 803	$Z_4 \rightarrow B_4$	241	
	3595.2*	0.04	27 808	$Z_3 \rightarrow B_3$	215	
	3592.6*	0.02	27 828	$Z_5 \rightarrow B_5$	247	
	3591.6*	0.03	27 835	$Z_4 \rightarrow B_5$	240	
	3589.6*	0.12	27 850	$Z_2 \rightarrow B_2$	27	
	3588.4*	0.03	27 859	$Z_3 \rightarrow B_5$	216	
	3587.3[g]	0.15	27 868	$Z_1 \rightarrow B_1$	0	1(*b*,*e*)
	3586.2[g]	0.32	27 877	$Z_1 \rightarrow B_2$	0	3(*b*,*e*)
	3570.8*	0.80	27 996	$Z_2 \rightarrow B_3$	27	
	3568.2*	0.45	28 017	$Z_2 \rightarrow B_4$	27	
			(28 023)	(B_3)		2(*d*,*e*)
	3564.8[g]	0.25	28 044	$Z_1 \rightarrow B_4$	0	4(*b*,*e*)

TABLE III. (*Continued*).

$^{2S+1}L_J$	λ (Å)[a]	I	E (cm^{-1})[b]	Trans.[c]	E (cm^{-1})[d]	Γ_n^e
	3560.8[g]	0.90	28 075	$Z_1 \rightarrow B_5$	0	1(*b*,*e*)
	3560.5[g]	0.70	28 078	shoulder		
$^1I_6$	2927.4*	0.01	34 150	$Z_4 \rightarrow C_1$	241	
	2925.3*	0.02	34 175	$Z_3 \rightarrow C_1$	216	
	2921.0*	0.02	34 225	$Z_3 \rightarrow C_3$	215	
	2920.2*	0.02	34 234	$Z_3 \rightarrow C_4$	215	
	2916.3*	0.02	34 280	$Z_4 \rightarrow C_5$	240	
	2907.0	0.10	34 391	$Z_1 \rightarrow C_1$	0	1(*b*,*e*)
	2906.6*(sh)	0.03	34 395	$Z_2 \rightarrow C_2$	27	
	2905.0*(sh)	0.04	34 413	$Z_2 \rightarrow C_3$	27	
	2904.1	0.09	34 422	$Z_1 \rightarrow C_2$	0	4(*b*,*e*)
			(34 440)	(C_3)		2(*d*,*e*)
	2902.0	0.20	34 449	$Z_1 \rightarrow C_4$	0	3(*b*,*e*)
	2898.3*	0.03	34 493	$Z_2 \rightarrow C_5$	27	
	2896.0	0.02	34 520	$Z_1 \rightarrow C_5$	0	4(*b*,*e*)
	2877.0[f]	0.01	34 748	$Z_1 \rightarrow C_7$	0	
	2855.4[f]	0.01	35 033	$Z_1 \rightarrow C_9$	0	1(*b*,*e*)
$^3P_0$	2846.1*	0.02	35 125	$Z_5 \rightarrow D_1$	247	
	2845.6*	0.02	35 132	$Z_4 \rightarrow D_1$	240	
	2843.6*	0.02	35 156	$Z_3 \rightarrow D_1$	216	
	2826.3	0.15	35 372	$Z_1 \rightarrow D_1$	0	1(*b*,*e*)
$^3P_1$	2778.0*	0.02	35 987	$Z_5 \rightarrow E_1$	247	
	2775.6*	0.01	36 018	$Z_3 \rightarrow E_1$	216	
	2765.5*	0.01	36 149	$Z_4 \rightarrow E_2$	242	
	2763.4*	0.02	36 177	$Z_4 \rightarrow E_3$	241	
	2761.1*	0.02	36 207	$Z_2 \rightarrow E_1$	27	
	2759.0	0.14	36 234	$Z_1 \rightarrow E_1$	0	3(*b*,*e*)
	2751.9	0.02	36 327			
	2749.0*	0.03	36 364	$Z_2 \rightarrow E_2$	27	
	2747.1	0.08	36 391	$Z_1 \rightarrow E_2$	0	4(*b*,*e*)
	2745.1	0.17	36 418	$Z_1 \rightarrow E_3$	0	
$^3P_2$	2652.8*	0.01	37 685	$Z_5 \rightarrow F_1$	247	
	2650.7*	0.01	37 715	$Z_3 \rightarrow F_1$	217	
	2643.5*	0.02	37 819	$Z_5 \rightarrow F_2$	247	
	2643.0*	0.02	37 826	$Z_4 \rightarrow F_2$	240	
	2641.2*	0.02	37 851	$Z_5 \rightarrow F_3$	247	
	2639.0*	0.03	37 881	$Z_3 \rightarrow F_3$	217	
	2637.4*	0.03	37 905	$Z_2 \rightarrow F_1$	27	
	2635.5	0.08	37 932	$Z_1 \rightarrow F_1$	0	3(*b*,*e*)
	2628.0*(sh)	0.05	38 039	$Z_2 \rightarrow F_2$	27	
	2626.2	0.86	38 066	$Z_1 \rightarrow F_2$	0	4(*b*,*e*)
	2624.0	0.48	38 098	$Z_1 \rightarrow F_3$	0	1(*b*,*e*)
	2620.0*	0.03	38 157	$Z_4 \rightarrow F_4$	241	
	2618.2*	0.03	38 182	$Z_3 \rightarrow F_4$	216	
	2617.1*	0.03	38 199	$Z_4 \rightarrow F_5$	241	
	2615.3*	0.04	38 224	$Z_3 \rightarrow F_5$	216	
	2611.2[f]	0.04	38 285			
	2605.3*	0.07	38 371	$Z_2 \rightarrow F_4$	(27)	
			(38 398)	(F_4)		2(*d*,*e*)
	2600.7[f]	0.63	38 440	$Z_1 \rightarrow F_5$	0	1(*b*,*e*)

[a]Temperature-dependent (hot-band) transitions are denoted by *, which are established by comparison with 90-K absorption spectrum. sh denotes shoulder.

[b]Transitions in vacuum wave numbers; values in parentheses deduced from hot bands.

[c]Transitions assigned to absorption spectrum of Tm^{3+} in sites of D_2 symmetry.

[d]Experimental level for initial state deduced from transition to final state.

[e]D_2 symmetry representations Γ_1, Γ_2, Γ_3, and Γ_4; letters in parentheses refer to method of assignment given in Sec. III.

[f]Band containing one or more shoulders.

[g]Lines or bands that persist at 1.6 K.

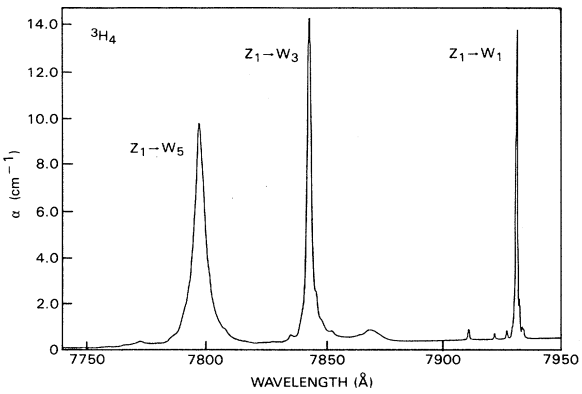

FIG. 1. Absorption spectrum of part of the $^3H_4$ manifold observed at 1.6 K. Weak peaks observed between 7910 and 7940 Å are presumed to be due to Tm^{3+} ions in minority sites.

weak electronic transitions to two Stark levels predicted at 684 and 698 cm^{-1}.

Using similar methods, we examined laser-excited emission from Stark levels in other manifolds including $^3H_4(\Gamma_1)$ at 12 607 cm^{-1}, $^1G_4(\Gamma_1)$ at 20 805 cm^{-1}, and $^1G_4(\Gamma_3)$ at 21 227 cm^{-1}. Emission from the Γ_1 levels was similar to that observed from $^3F_4(\Gamma_1)$ in Fig. 9. Transitions to levels identified as Γ_1 in absorption at 27 cm^{-1} and 252 cm^{-1} were absent. Figure 10 shows part of the emission spectrum from the $^1G_4(\Gamma_1)$ level at 20 805 cm^{-1}. The emission spectra from the $^1D_2$ manifold to $^3H_6$, $^3F_4$, $^3F_3$, and $^3F_2$ were more difficult to analyze. The crystal was excited at 3547 Å where absorption is observed due

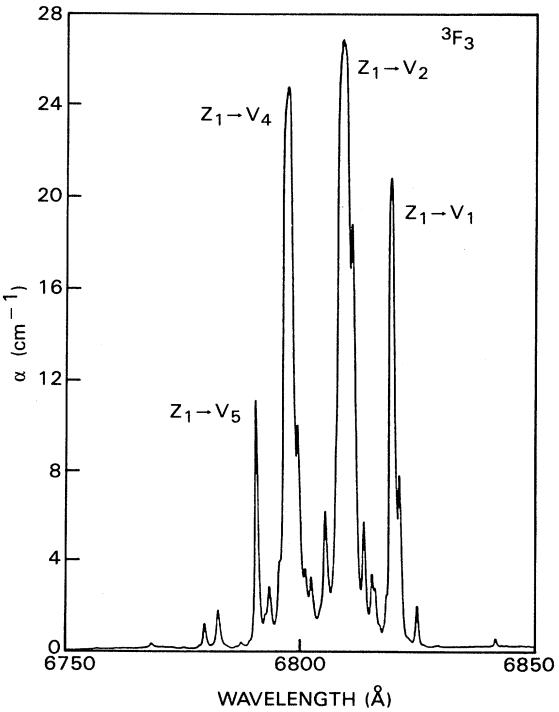

FIG. 2. Absorption spectrum of the $^3F_3$ manifold observed at 1.6 K.

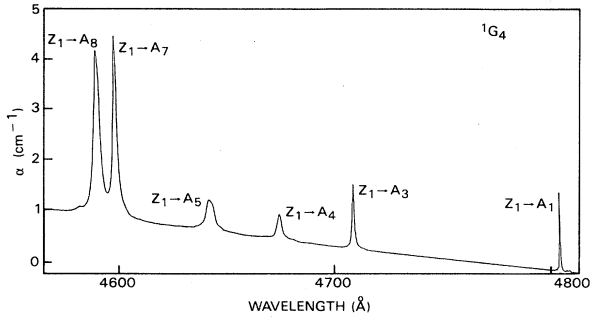

FIG. 3. Absorption spectrum of the $^1G_4$ manifold observed at 1.6 K.

to a phonon sideband of the highest energy Stark level in $^1D_2$ (B_5 at 3561 Å). All Stark levels of $^1D_2$ appear to fluoresce to the $^3H_6$ manifold (see Fig. 11). If we assume the experimental splitting of $^3H_6$ as determined from the previous analyses of the absorption and emission spectra, the five bands can be identified in Fig. 11. A similar approach can be used to identify the structure in Figs. 12 and 13.

VI. CRYSTAL-FIELD SPLITTING CALCULATIONS

The free-ion wave functions were determined using a Hamiltonian that contained the Coulombic interactions in the form of the Racah parameters $E^{(1)}$, $E^{(2)}$, and $E^{(3)}$, and the spin-orbit parameter ζ. The generalized Trees' interconfiguration interaction was also included in the form of parameters α, β, and γ.[26] We chose the following set of parameters for our calculation: $E^{(1)}=7142.4$, $E^{(2)}=33.795$, $E^{(3)}=674.27$, $\zeta=2628.7$, $\alpha=14.677$, $\beta=-631.79$, $\gamma=0$, all in cm^{-1}.[27]

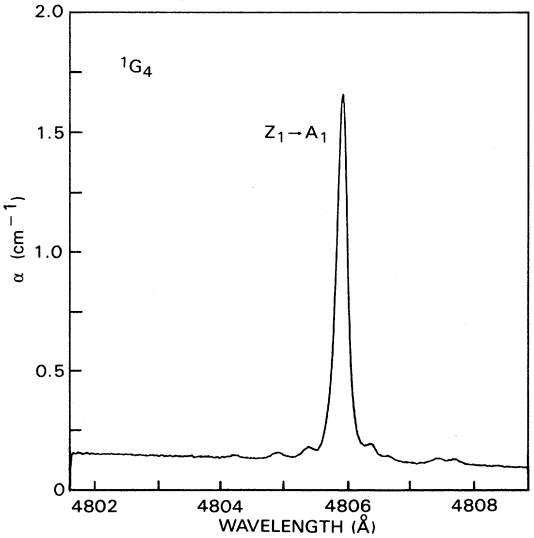

FIG. 4. Absorption spectrum of the $Z_1 \rightarrow A_1$ transition in the $^1G_4$ manifold observed at 1.6 K. As many as six very weak peaks are found clustered around the strong peak.

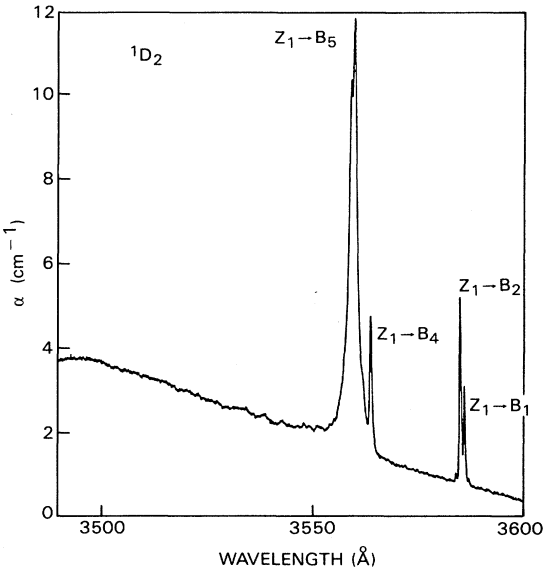

FIG. 5. Absorption spectrum of the $^1D_2$ manifold observed at 1.6 K.

A crystal-field splitting Hamiltonian having D_2 symmetry was taken in the form of

$$H_{\mathrm{CEF}} = \sum_{n,m} B_{nm}^{+} \sum_{i} C_{nm}(\hat{\mathbf{r}}_i) , \tag{1}$$

where B_{nm} represent the crystal-field splitting parameters and the complex conjugate satisfies the relation

$$B_{nm}^{+} = (-1)^m B_{n,-m} . \tag{2}$$

The expressions $C_{nm}(\hat{\mathbf{r}})$ in Eq. (1) are related to the standard spherical harmonics through the expression

$$C_{nm}(\hat{\mathbf{r}}) = [4\pi/(2n+1)]^{1/2} Y_{n,m} . \tag{3}$$

The wave function chosen for a basis for the calculation of the crystal field is given in Ref. 4. The free-ion wave functions, using the parameters given earlier, were used to calculate the matrix elements of the crystal field of Eq. (1).

To establish a set of B_{nm} parameters that could be related to a physical model we first carried out a lattice-sum calculation that included point-charge, point-dipole, and self-induced contributions.[28] The ion positions in the garnet lattice, effective ionic electric charges, and the polarizability of the oxygen ions are given in Ref. 4. The calculated lattice-sum parameters A_{nm} are related to the B_{nm} parameters through the radial factors ρ_n for the Tm^{3+} ion as follows:

$$B_{nm} = \rho_n(\mathrm{Tm}) A_{nm} , \tag{4}$$

where

$$\rho_2 = 0.1722, \quad \rho_4 = 0.4033, \quad \text{and} \quad \rho_6 = 0.9649 . \tag{5}$$

For Tm^{3+} ions occupying $Y^{3+}(D_2)$ sites in the lattice, the nine B_{nm} parameters obtained from the lattice-sum calculation are $B_{20}=250$, $B_{22}=382$, $B_{40}=-248$, $B_{42}=-1133$, $B_{44}=-1990$, $B_{60}=-1426$, $B_{62}=-548$, $B_{64}=526$, $B_{66}=-484$, all in cm^{-1}. Using these parameters in the crystal-field splitting calculation, we obtained theoretical Stark levels in reasonable agreement with the overall splitting for each J manifold as determined from experiment. A particularly helpful outcome of this calculation and all subsequent calculations was the prediction

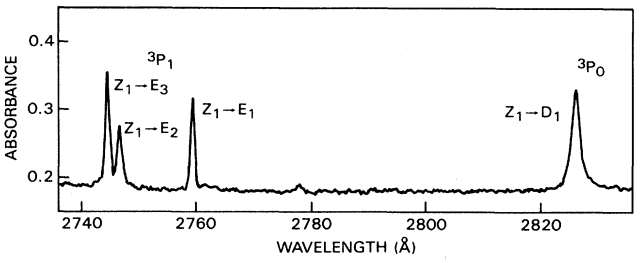

FIG. 7. Absorption spectrum of the $^3P_0$ and $^3P_1$ manifolds at 15 K.

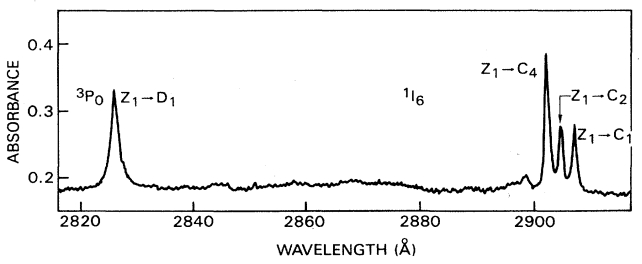

FIG. 6. Absorption spectrum of the $^1I_6$ and $^3P_0$ manifolds at 15 K.

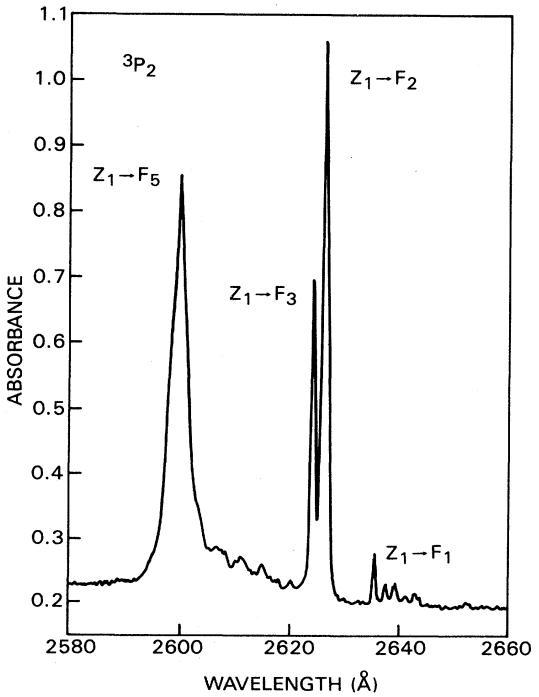

FIG. 8. Absorption spectrum of the $^3P_2$ manifold at 15 K.

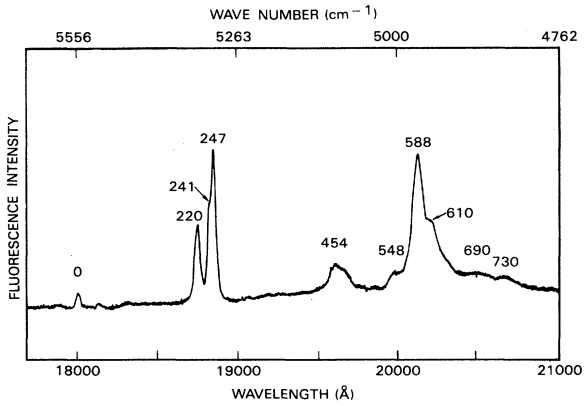

FIG. 9. Fluorescence from $^3F_4$ (5556-cm^{-1} level) to $^3H_6$ at 80 K with associated terminal levels shown in cm^{-1} beside observed peaks.

that the ground state Z_1 had Γ_2 symmetry. Our analyses of experimental data were consistent with this prediction.

A second crystal-field splitting calculation was performed using a set of B_{nm} parameters obtained from a quadratic fit to the empirical B_{nm} parameters that were established by fitting the experimental data of several other R^{3+} ions in YAG.[28] This set of B_{nm} parameters calculated for Tm^{3+} from the quadratic fit are $B_{20}=372$, $B_{22}=85$, $B_{40}=-301$, $B_{42}=-1540$, $B_{44}=-948$, $B_{60}=-1082$, $B_{62}=-258$, $B_{64}=477$, $B_{66}=-240$, all in cm^{-1}. The calculated splitting and predicted symmetry assignments agreed well enough with the experimental analysis that we allowed the centroids (center of gravity) of each J manifold along with the crystal-field parameters B_{nm} to vary freely to obtain the best overall agreement between 66 calculated and observed Stark levels. The results of that calculation and the final set of B_{nm} parameters are given in Table V. The rms deviation between 66 experimental and calculated Stark levels is 11 cm^{-1}. Each $^{2S+1}L_J$ manifold label is based on the free-ion state having the largest composition in Russell-Saunders coupling. The percent composition given in Table V indicates the mixtures caused by the crystal field.

VII. DISCUSSION

The calculated splitting of the $^3H_6$ manifold in Table V is in reasonable agreement with Stark levels established from absorption and emission data. The symmetry of each calculated level is also compared with the symmetry deduced from the analysis in Sec. III. In the $^3H_6$ manifold the symmetry of Z_5 is probably Γ_2 from the analysis of transitions to and from that level. The limited number of transitions from Z_6 is consistent with the assignment of Γ_1 symmetry. Laser-excited emission spectra establish additional Stark levels at 588 and 610 cm^{-1} with the less certain possibilities at 690 and 730 cm^{-1}.

Stark levels Y_1 through Y_7 ($^3F_4$, Table III) can be associated directly with the calculated splitting and predicted symmetry labels given in Table V. Hot-band data associated with isolated Stark levels Y_1, Y_2, and Y_4 were useful in determining the splitting and symmetry assignments to Stark levels within the $^3H_6$ manifold. The Γ_2 levels, Y_3 and Y_6, were inferred from the hot-band data and confirmed in emission (Fig. 12). The absorption peak at 6143 cm^{-1} shows no evidence of temperature dependence. Because of its shape and structure, it is presumed to be vibronic in origin. The strong peak at 6170 cm^{-1} has Γ_1 symmetry in agreement with the calculation. Assignments to levels Y_8 and Y_9 are based on the predicted splitting. Analysis of the fluorescence in Fig. 12 supports the assignments given to experimental Stark levels listed in Table V.

Six Stark levels within the $^3H_5$ manifold were identified from the data. Levels X_1 and X_2 are sufficiently isolated from the rest of the manifold so that transitions to these

TABLE IV. Emission from $^3F_4$ (5556 cm^{-1}, Γ_1) to the $^3H_6$ manifold (measured at 80 K).

Emission λ (μm)	Trans. $Y_1 \rightarrow Z_n$	Energy (cm^{-1})	Splitting $^3H_6$ emission (cm^{-1})	Splitting $^3H_6$ abs.[a] (cm^{-1})	Γ_n expt.	Splitting $^3H_6$ calc.[b] (cm^{-1})	Γ_n calc.
1.800	$Y_1 \rightarrow Z_1$	5556	0	0	Γ_2	−3	Γ_2
				27	Γ_1	24	Γ_1
1.874	$Y_1 \rightarrow Z_3$	5336	220	216	Γ_4	215	Γ_4
1.882	$Y_1 \rightarrow Z_4$	5315	241	241	Γ_3	225	Γ_3
1.884	$Y_1 \rightarrow Z_5$	5309	247	247	Γ_2	262	Γ_2
				252	Γ_1	253	Γ_1
1.960		5102	454				
1.997		5008	548				
2.013		4968	588			518	Γ_4
2.022		4946	610			610	Γ_3
						650	Γ_1
2.055		4866	690			684	Γ_2
						698	Γ_4
2.072		4826	730			751	Γ_3
						765	Γ_1

[a]Hot-band absorption, Table III.
[b]Crystal-field parameters and calculation, Table V.

TABLE V. Energy levels of Tm^{3+} ions in D_2 sites.

$^{2S+1}L_J$	E (cm^{-1}) expt.[a]	Γ_n expt.[a]	E (cm^{-1}) calc.[b]	Γ_n calc.[b]	Free-ion mixture (%)
$^3H_6$	0	2	−3	2	$99.8\,^3H_6+0.1\,^3F_4+0.1\,^3F_3$
	27	1	24	1	$99.7\,^3H_6+0.2\,^3F_4$
	216	4	215	4	$99.7\,^3H_6+0.2\,^3F_4+0.1\,^3F_3$
	241	3	225	3	$99.5\,^3H_6+0.3\,^3F_4$
	247	...	262	2	$99.5\,^3H_6+0.4\,^3F_4+0.1\,^3H_4$
456[c]	252	1	253	1	$99.9\,^3H_6+0.1\,^3F_4$
	588[d]	...	518	4	$99.6\,^3H_6+0.2\,^3F_4+0.1\,^3H_5$
	610[d]	...	610	3	$99.9\,^3H_6+0.1\,^3H_5$
	...	...	650	1	$99.7\,^3H_6+0.3\,^3F_4$
	690[d]	...	684	2	$99.5\,^3H_6+0.4\,^3F_4+0.1\,^3H_5$
	...	...	698	4	$99.8\,^3H_6+0.1\,^3F_4+0.1\,^3H_5$
	730[d]	...	751	3	$99.8\,^3H_6+0.2\,^3F_4+0.1\,^3H_5$
	...	...	765	1	$99.7\,^3H_6+0.2\,^3F_4+0.1\,^3H_5$
$^3F_4$	5556	1	5536	1	$99.2\,^3F_4+0.4\,^3H_5+0.2\,^3H_4$
	5736	3	5757	3	$98.5\,^3F_4+1.2\,^3H_5+0.3\,^3H_6$
	5832	2	5810	2	$98.5\,^3F_4+1.1\,^3H_5+0.4\,^3H_6$
	5901	4	5912	4	$98.6\,^3F_4+1.0\,^3H_5+0.4\,^3H_6$
5986[c]	6041	1	6040	1	$99.3\,^3F_4+0.4\,^3H_6+0.2\,^3H_5$
	6108	2	6111	2	$99.5\,^3F_4+0.3\,^3H_5+0.2\,^3H_6$
	6170	1	6164	1	$99.3\,^3F_4+0.4\,^3H_5+0.2\,^3H_6$
	6224	...	6228	4	$99.3\,^3F_4+0.4\,^3H_5+0.2\,^3H_6$
	6233	...	6243	3	$99.6\,^3F_4+0.3\,^3H_6+0.1\,^3H_5$
$^3H_5$	8339	4	8343	4	$99.0\,^3H_5+0.7\,^3F_4+0.2\,^3F_2$
	8345	3	8353	3	$99.3\,^3H_5+0.4\,^3F_4+0.1\,^3F_2$
	8516	3	8507	3	$98.8\,^3H_5+0.8\,^3F_4+0.2\,^3H_4$
	8530	1	8517	1	$98.8\,^3H_5+0.6\,^3F_4+0.4\,^3F_2$
	...	...	8524	2	$98.6\,^3H_5+1.1\,^3F_4+0.2\,^3F_3$
	8556	4	8558	4	$98.9\,^3H_5+0.8\,^3F_4+0.1\,^3F_3$
8631[c]	8711	2	8712	2	$99.0\,^3H_5+0.7\,^3H_4+0.2\,^3F_4$
	8773	...	8774	1	$99.1\,^3H_5+0.7\,^3H_4+0.1\,^3F_4$
	8800	...	8804	3	$99.5\,^3H_5+0.3\,^3F_3+0.2\,^3H_4$
	...	...	8873	2	$99.3\,^3H_5+0.6\,^3H_4+0.1\,^3F_4$
	8882	...	8885	4	$99.4\,^3H_5+0.3\,^3H_4+0.2\,^3F_3$
$^3H_4$	12 607	1	12 614	1	$98.0\,^3H_4+1.1\,^3F_2+0.8\,^3H_5$
	12 679	2	12 677	2	$97.1\,^3H_4+1.9\,^3F_3+0.6\,^3H_5$
	12 747	4	12 749	4	$96.5\,^3H_4+3.0\,^3F_3+0.5\,^3H_5$
	...	...	12 818	2	$98.1\,^3H_4+0.8\,^3F_2+0.7\,^3H_5$
	12 824	3	12 832	3	$96.8\,^3H_4+2.6\,^3F_3+0.4\,^3H_5$
12 909[c]			12 954	1	$99.4\,^3H_4+0.2\,^3F_3+0.2\,^3F_4$
	13 072	4	13 070	4	$98.7\,^3H_4+1.0\,^3F_3+0.3\,^3F_2$
	13 139	3	13 127	3	$98.9\,^3H_4+1.0\,^3F_3+0.1\,^3F_4$
	13 159	...	13 159	1	$98.1\,^3H_4+1.6\,^3F_3+0.2\,^3F_2$
$^3F_3$	14 659	4	14 643	4	$94.3\,^3F_3+2.8\,^3F_2+2.7\,^3H_4$
	...	...	14 649	2	$97.8\,^3F_3+1.8\,^3H_4+0.2\,^3H_5$
	...	...	14 661	2	$99.2\,^3F_3+0.5\,^3H_4+0.1\,^3F_2$
14 665[c]	14 679	3	14 683	3	$95.6\,^3F_3+2.4\,^3H_4+1.6\,^3F_2$
	14 705	...	14 710	4	$96.7\,^3F_3+1.5\,^3H_4+1.5\,^3F_2$
	14 720	...	14 730	3	$90.0\,^3F_3+8.5\,^3F_2+1.2\,^3H_4$
	14 741	1	14 737	1	$93.8\,^3F_3+4.1\,^3F_2+1.9\,^3H_4$
$^3F_2$	15 245	3	15 246	3	$89.3\,^3F_2+10.2\,^3F_3+0.3\,^3H_4$
	15 264	4	15 260	4	$95.0\,^3F_2+4.6\,^3F_3+0.1\,^3H_5$
15 293[c]	...	...	15 302	1	$96.8\,^3F_2+2.4\,^3F_3+0.4\,^3H_4$
	...	...	15 433	2	$98.5\,^3F_2+1.1\,^3H_4+0.2\,^3F_3$
	15 438	1	15 440	1	$96.9\,^3F_2+1.9\,^3F_3+1.0\,^3H_4$
$^1G_4$	20 805	1	20 815	1	$99.6\,^1G_4+0.3\,^1I_6+0.1\,^3H_4$

TABLE V. (*Continued*).

$^{2S+1}L_J$	E (cm^{-1}) expt.[a]	Γ_n expt.[a]	E (cm^{-1}) calc.[b]	Γ_n calc.[b]	Free-ion mixture (%)
	...	...	21 191	2	$99.8\,^1G_4+0.1\,^1I_6+0.1\,^3F_3$
	21 227	3	21 225	3	$99.7\,^1G_4+0.1\,^1I_6+0.1\,^3F_3$
	21 381	4	21 387	4	$99.8\,^1G_4+0.1\,^1I_6+0.1\,^3F_3$
21 483[c]	21 530	1	21 513	1	$99.7\,^1G_4+0.1\,^1D_2+0.1\,^3F_2$
	21 687	2	21 681	2	$99.7\,^1G_4+0.1\,^1D_2+0.1\,^3F_2$
	21 757	1	21 767	1	$100.0\,^1G_4$
	...	...	21 824	4	$99.9\,^1G_4+0.1\,^1D_2$
	...	...	21 864	3	$100.0\,^1G_4$
$^1D_2$	27 868	1[e]	27 914	1	$99.7\,^1D_2+0.2\,^1G_4+0.1\,^3F_2$
	27 877	3[e]	27 940	3	$99.7\,^1D_2+0.2\,^1I_6$
27 995[c]	28 023	2	28 027	2	$99.8\,^1D_2+0.1\,^1G_4$
	28 044	4	28 048	4	$99.6\,^1D_2+0.2\,^1I_6+0.1\,^1G_4$
	28 075	1	28 067	1	$99.7\,^1D_2+0.2\,^1I_6+0.1\,^1G_4$
$^1I_6$	34 391	1	34 380	1	$99.1\,^1I_6+0.4\,^3P_0+0.2\,^1G_4$
	34 422	4	34 424	4	$99.9\,^1I_6+0.1\,^1G_4$
	34 440	2	34 446	2	$99.8\,^1I_6+0.1\,^1G_4$
	34 449	3	34 449	3	$99.3\,^1I_6+0.5\,^3P_2+0.2\,^1D_2$
	34 520	4	34 522	4	$99.1\,^1I_6+0.6\,^3P_2+0.2\,^1D_2$
	...	...	34 679	3	$99.7\,^1I_6+0.1\,^3P_2+0.1\,^1G_4$
	34 748	1[e]	34 726	1	$99.4\,^1I_6+0.4\,^3P_2+0.1\,^1D_2$
34 832[c]	35 033	1	35 034	1	$99.9\,^1I_6+0.1\,^3P_0$
	...	...	35 034	2	$100.0\,^1I_6$
	...	...	35 204	2	$100.0\,^1I_6$
	...	...	35 227	4	$99.9\,^1I_6+0.1\,^3P_2$
$^3P_0$	35 372	1	35 372	1	$97.7\,^3P_0+2.1\,^1I_6+0.1\,^3P_2$
35 357[c]					
$^1I_6$	...	...	35 387	3	$99.8\,^1I_6+0.1\,^3P_2$
	...	...	35 399	1	$98.2\,^1I_6+1.6\,^3P_0+0.1\,^3P_2$
$^3P_1$	36 234	3	36 254	3	$99.9\,^3P_1$
36 336[c]	36 391	4	36 381	4	$99.6\,^3P_1+0.3\,^3P_2$
	36 418	2	36 408	2	$99.8\,^3P_1+0.2\,^3P_2$
$^3P_2$	37 932	3	37 935	3	$99.2\,^3P_2+0.8\,^1I_6$
	38 066	4	38 000	4	$98.9\,^3P_2+0.7\,^1I_6+0.4\,^3P_1$
38 140[c]	38 098	1	38 088	1	$99.4\,^3P_2+0.5\,^1I_6$
	38 398	2	38 402	2	$99.8\,^3P_2+0.2\,^3P_1$
	38 440	1	38 409	1	$99.6\,^3P_2+0.2\,^1I_6+0.1\,^3P_0$
$^1S_0$			79 604	1	$100.0\,^1S_0$
79 592[c]					

[a]Levels obtained from Tables III and IV; hot bands used to assign symmetry representations Γ_n; ellipses indicate Γ_n was not established from experimental data.

[b]Levels calculated using crystal-field parameters $B_{20}=474\ cm^{-1}$, $B_{22}=47.0\ cm^{-1}$, $B_{40}=-213\ cm^{-1}$, $B_{42}=-1571\ cm^{-1}$, $B_{44}=-824\ cm^{-1}$, $B_{60}=-984\ cm^{-1}$, $B_{62}=-310\ cm^{-1}$, $B_{64}=591\ cm^{-1}$, and $B_{66}=-193\ cm^{-1}$; rms deviation between 66 experimental levels with symmetry labels and calculated levels is 11 cm^{-1}.

[c]Centroid for the $^{2S+1}L_J$ manifold.

[d]For purposes of the calculation only, these levels were assigned tentative symmetry labels: 588 (Γ_4), 610 (Γ_3), 690 (Γ_2), and 730 (Γ_3), all in cm^{-1}; 548 and 588 cm^{-1} were used in the calculation in place of experimental levels 588 and 610 cm^{-1}.

[e]Levels not included in final fitting procedure.

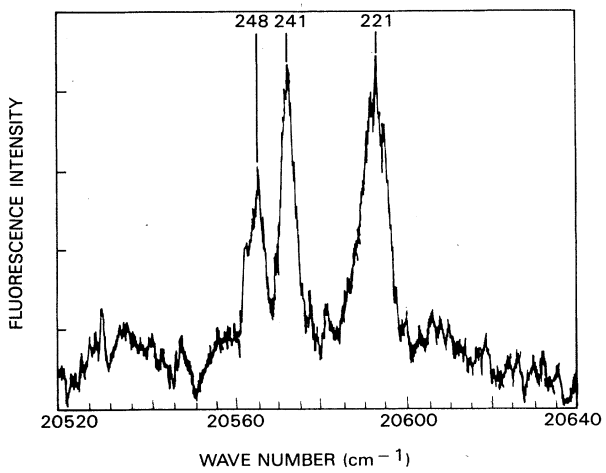

FIG. 10. Part of the fluorescence from $^1G_4$ (20 805-cm^{-1} level) to $^3H_6$ at 80 K with associated terminal levels shown in cm^{-1} beside observed peaks.

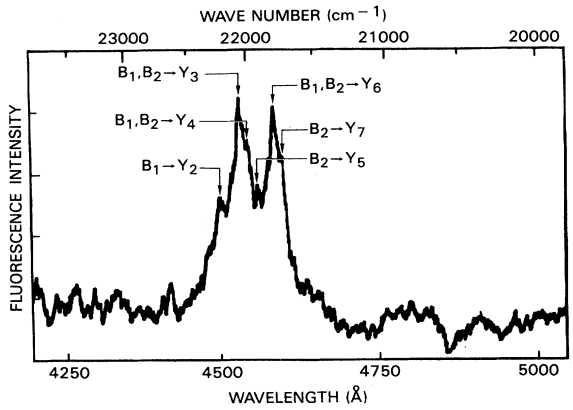

FIG. 12. Fluorescence from $^1D_2$ to $^3F_4$ at 80 K.

levels from Z_1 through Z_6 could be identified. A Γ_2 level is predicted at 8524 cm^{-1} (Table V) which is close to levels $X_3(\Gamma_3)$ at 8516 cm^{-1} and $X_4(\Gamma_1)$ at 8530 cm^{-1} that have been identified from observed hot-band data (Table III). From a shoulder on the strong hot band at 8489 cm^{-1} we may infer a Γ_2 level around 8520 cm^{-1}. The higher energy absorption peaks within the manifold are broadened due to spontaneous phonon decay making it difficult to locate and identify the remaining Stark levels. Levels X_8, X_9, and X_{11} were associated with the predicted splitting and symmetry labels obtained from the final crystal-field splitting calculation.

Out of nine expected Stark levels for $^3H_4$ we have identified six by analyzing the observed hot-band spectra. The absorption spectra recorded at 1.6 K (Fig. 1) shows no evidence of the 27-cm^{-1} hot bands that still persist in the 15-K absorption spectrum. The level W_1 at 12 607 cm^{-1} was examined in both emission and absorption and found to have Γ_1 symmetry as predicted by the calculation. A very weak peak is observed at 12 679 cm^{-1}. A Γ_2 Stark level is predicted at 12 677 cm^{-1}. Selection rules forbid $\Gamma_2 \rightarrow \Gamma_2$ transitions. The peak may be due to Tm^{3+} ions in one of the minority sites. The shape of the peak also suggests that it may be vibronic in origin. A strong hot band at 12 797 cm^{-1} (Table III), assigned as a $Z_2 \rightarrow W_5$ transition, has a pronounced shoulder that could be used to predict a Γ_2 level at 12 820 cm^{-1}, in agreement with a calculated value of 12 818 cm^{-1}. A broad band with structure centered at 13 159 cm^{-1} may include the Stark level predicted at 13 159 cm^{-1}.

The 1.6-K absorption spectrum of the $^3F_3$ manifold (Fig. 2) contains so many closely spaced peaks of varying intensity, that only a few Stark levels could be identified without ambiguity. At 1.6 K, transitions from $Z_1(\Gamma_2)$ to the two excited Γ_2 Stark levels within $^3F_3$ are forbidden. The most intense peaks should represent transitions from Z_1 to the expected 2 Γ_4, 2 Γ_3, and 1 Γ_1 Stark levels. From hot-band data we have identified levels at 14 659(V_1) and 14 679(V_2) cm^{-1} as having Γ_4 and Γ_3 symmetry, respectively. On the basis of the most intense peaks observed at 1.6 K (Fig. 2) and the calculated splitting, we can infer levels at 14 705 and 14 720 cm^{-1} as

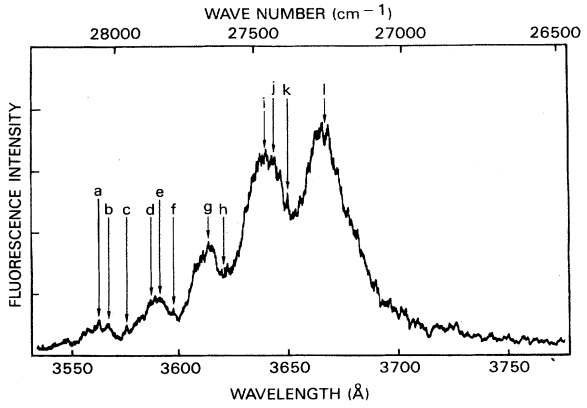

FIG. 11. Fluorescence from $^1D_2$ to $^3H_6$ at 80 K. Arrows mark positions where peaks are expected based on levels determined from absorption: *a*, $B_5 \rightarrow Z_1$; *b*, $B_4 \rightarrow Z_1$; *c*, $B_3 \rightarrow Z_2$; *d*, $B_1,B_2 \rightarrow Z_1$; *e*, $B_2 \rightarrow Z_2$; *f*, $B_3 \rightarrow Z_4$; *g*, $B_1,B_2 \rightarrow Z_3$; *h*, $B_1,B_2 \rightarrow Z_4,Z_5$; *i*, $B_5 \rightarrow Z_8$; *j*, $B_4 \rightarrow Z_8$; *k*, $B_5 \rightarrow Z_8$; and *l*, $B_1 \rightarrow Z_8$.

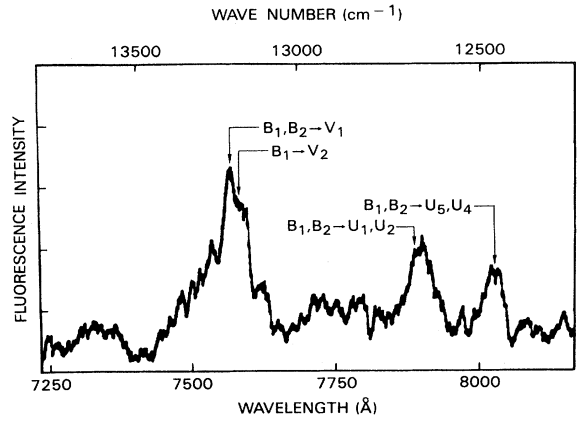

FIG. 13. Fluorescence from $^1D_2$ to $^3F_3$ and $^3F_2$ at 80 K.

having Γ_4 and Γ_3 symmetry, respectively. The remaining allowed transition from the ground state appears to be much weaker; the level at 14 741 cm^{-1} has hot bands that indicate it has Γ_1 symmetry. The emission spectrum (Fig. 13) is consistent with these assignments.

From experiment, three out of five and six out of nine possible Stark levels were assigned within the $^3F_2$ and $^1G_4$ (Fig. 3) manifolds, respectively. The isolated level at 20 805 cm^{-1} was examined in both emission and absorption and found to have Γ_1 symmetry in agreement with the calculation. The Γ_2 level predicted at 21 191 cm^{-1} (Table V) could not be verified from experiment since the hot bands associated with that level could not be distinguished from weak spectra possibly due to Tm^{3+} ions in minority sites. Absorption at 1.6 K (Fig. 3) between 21 785 and 21 840 cm^{-1} may be associated with the two highest energy Stark levels predicted by the calculation. The observed overall splitting of the $^1G_4$ manifold is in very good agreement with the calculated total splitting which is more than 1000 cm^{-1}.

Hot-band data associated with the $^1D_2$ manifold (Table III) were useful in establishing the symmetry of all five Stark levels and reaffirmed symmetry assignments to levels Z_1 through Z_5 established from analyses of hot-band data to other excited manifolds. Although every calculation which included the five experimental levels in the fitting routine correctly predicted the symmetry for each level, it was not possible to obtain agreement between the overall calculated and observed manifold splitting. It is possible that levels B_1 and B_2 are relatively more sensitive than B_3, B_4, and B_5 to atomic interactions not included in our Hamiltonian. In the final calculation B_1 and B_2 were not included in the fitting routine in order to obtain the best overall agreement between B_3, B_4, B_5, and Stark levels from other manifolds.

The predicted overall splitting of the $^1I_6$ manifold is roughly 1000 cm^{-1}. Our experiments indicate that the five calculated lowest-energy Stark levels can be correlated with the reasonably strong sharp spectra used to identify levels C_1 through C_5 (Fig. 6). A number of weak peaks were not assigned to a particular transition since they may arise from Tm^{3+} ions in minority sites. The calculation (Table V) predicts that the two highest energy Stark levels of the $^1I_6$ manifold overlap the predicted energy for the $^3P_0$ level by a small amount. The very weak broad absorption in the vicinity of the relatively strong sharp absorption peak identified as the $^3P_0$ may be due to $^1I_6$ absorption. We analyzed only the strongest hot bands in this region; $^3P_0$ in assigned to the level at 35 372 cm^{-1}.

Several ambiguities in the analysis of the $^3P_1$ and $^3P_2$ manifolds (Table III) could not be resolved. The peak at 2747 Å has a temperature-dependent shoulder that may be an unresolved (27 cm^{-1}) hot band to the 2745 Å peak. Spectra at 90 K clearly show hot bands that predict Stark levels at 36 391 cm^{-1} (2747 Å) and at 36 418 cm^{-1} (2745 Å). The calculation (Table V) predicts a Γ_4 level at 36 381 cm^{-1} and a Γ_2 level at 36 408 cm^{-1}. The experimental level at 36 391 cm^{-1} has hot bands consistent with the Γ_4 prediction. Since a $\Gamma_2 \rightarrow \Gamma_2$ transition is forbidden it may be that the observed absorption at 2745 Å is a transition to the Γ_4 Stark level with the peak observed at 2747 Å (36 391 cm^{-1}) representing a very strong temperature-dependent transition from Z_2. In $^3P_2$ we observe three strong peaks and a sharp but much weaker peak at 2635 Å. The weaker peak has hot bands which identify it as a Γ_3 Stark level at 37 932 cm^{-1}. A predicted Γ_3 level is found (Table V) at 37 935 cm^{-1}. The strong sharp peaks at 2624 and 2626 Å are probably due to Γ_4 and Γ_1 Stark levels, while the peak containing structure at 2600 Å includes transitions to the remaining Γ_1 and Γ_2 levels of the $^3P_2$ manifold.

In summary, from analyses of emission and absorption data a number of Stark levels have been identified with Tm^{3+} ions in D_2 sites. These levels were included in a crystal-field splitting calculation. The results given in Table V yield a rms deviation of 11 cm^{-1} between the experimental and calculated levels.

ACKNOWLEDGMENTS

The authors wish to thank Milan R. Kokta, of Union Carbide Corporation (Washougal, Washington), for providing the crystals. One of us (J.B.G.) wishes to thank the American Society for Engineering Education for its support. Two of us from Harry Diamond Laboratories (C.A.M. and G.A.T.) wish to thank R. G. Buser and A. Pinto of U.S. Army Night Vision and Electro-Optics Laboratories (Fort Belvoir, Virginia), for their encouragement and support. Three of us from the Naval Research Laboratory (G.J.Q., G.J.K., and L.E.) acknowledge the technical assistance from Annette Rosenbaum and Gregg Rosenblatt.

*Present address: Spectra-Physics, Inc., 1250 Middlefield Road, Mountain View, CA 94039-7013.

[1]M. A. Acharekar and M. M. Kaplan, Spectroscopy **2**, 32 (1987).

[2]J. A. Mares, J. Kubelka, and J. Kvapil, Czech J. Phys. B **36**, 1079 (1986).

[3]E. V. Antonov, Kh. S. Bagdasarov, N. A. Kazakov, N. A. Kulagin, and L. P. Podus, Kristallografiya **29**, 175 (1984) [Sov. Phys.—Crystallogr. **29**, 106 (1984)].

[4]C. A. Morrison and R. P. Leavitt, in *Handbook on the Physics and Chemistry of Rare Earths,* edited by K. A. Gschneidner, Jr. and L. Eyring (North-Holland, New York, 1982), Vol. 5.

[5]A. A. Kaminskii, *Laser Crystals* (Springer, New York, 1981).

[6]L. Esterowitz, in *Technical Digest, Tunable Solid State Lasers* (Optical Society of America, Washington, D.C., 1987), paper MB3-1.

[7]G. Huber, E. W. Duczynski, and K. Petermann, Ref. 6, paper MC-1.

[8]E. W. Duczynski, G. Huber, and P. Mitzscherlich, in *Tunable Solid State Lasers II,* edited by A. B. Budgor, L. Esterowitz, and L. G. DeShazer (Springer-Verlag, Berlin, 1986), p. 282.

[9]M. Bass, W. Q. Shi, R. Kurtz, M. Kota, and H. Diegl, Ref. 8,

p. 300.
[10]G. J. Kintz, R. Allen, and L. Esterowitz, in *Technical Digest, Conference on Lasers and Electro-Optics* (Optical Society of America, Washington, D.C., 1988), paper FB-2.
[11]G. Huber, P. Mitzscherlich, T. Y. Fan, and R. L. Byer, J. Lumin. **40**, 509 (1988).
[12]T. Y. Fan, G. Huber, R. L. Byer, and P. Mitzscherlich, IEEE J. Quantum Electron. **QE-24**, 924 (1988).
[13]C. A. Morrison, D. E. Wortman, and N. Karayianis, J. Phys. C **9**, 191 (1976).
[14]J. B. Gruber, M. E. Hills, M. Nadler, M. R. Kokta, and C. A. Morrison, Chem. Phys. **113**, 175 (1987).
[15]R. Bayerer, J. Heber, and D. Mateika, Z. Phys. B **64**, 201 (1986).
[16]J. B. Gruber, M. E. Hills, R. M. Macfarlane, C. A. Morrison, and G. A. Turner, Chem. Phys. **134**, 241 (1989).
[17]Yu. K. Voronko and A. A. Sobol, Phys. Status Solidi **27**, 257 (1975).
[18]J. B. Gruber, M. E. Hills, M. P. Nadler, and M. R. Kokta, Bull. Am. Phys. Soc. **31**, 244 (1986).
[19]R. A. Buchanan, J. J. Pearson, and G. F. Herrmann, Solid State Comm. **7**, 195 (1969).
[20]G. M. Zverev, G. Ya. Kilodnyi, and A. M. Onishchenko, Zh. Eksp. Teor. Fiz. **57**, 794 (1969) [Sov. Phys.—JETP **30**, 435 (1970)].
[21]B. M. Antipenko and Yu. V. Tomashevich, Opt. Spektrosk. **44**, 272 (1978) [Opt. Spectrosc. (USSR) **44**, 157 (1978)].
[22]J. A. Caird, L. G. DeShazer, and J. Nella, IEEE J. Quantum Electron. **QE-11**, 874 (1975).
[23]G. J. Quarles, A. Rosenbaum, G. Rosenblatt, and L. Esterowitz, in *Conference Proceedings, IEEE Lasers and Electro-Optics* (IEEE Lasers and Electro-Optics Society, Piscataway, NJ, 1988), pp. 335-336.
[24]S. Geller, Z. Kristallogr. **125**, 1 (1967).
[25]G. F. Koster, J. O. Dimmock, R. G. Wheeler, and H. Statz, *Properties of the Thirty-two Point Groups* (MIT Press, Cambridge, MA, 1963).
[26]C. A. Morrison, *Angular Momentum Theory Applied to Interactions in Solids,* Vol. 47 of *Lecture Notes in Chemistry* (Springer-Verlag, New York, 1988).
[27]W. T. Carnall, P. R. Fields, and K. Rajnak, J. Chem. Phys. **49**, 4412 (1968).
[28]D. E. Wortman, C. A. Morrison, and N. Karayianis, Harry Diamond Laboratories Report No. HDL-TR-1773 (1976) (unpublished).